Proceedings of the ASME 2024 51st Annual Review of Progress in Quantitative Nondestructive Evaluation QNDE2024 July 22-24, 2024, Denver, Colorado

QNDE2024-137228, Draft

PERIDYNAMICS BASED MODELING FOR INVESTIGATING THE EFFECT OF TOPOGRAPHY AND TOPOLOGICAL ACOUSTIC SENSING PERFORMANCE IN MONITORING DAMAGE GROWTH

Guangdong Zhang University of Arizona Tucson, AZ Pierre A. Deymier University of Arizona Tucson, AZ Keith Runge University of Arizona Tucson, AZ **Tribikram Kundu**University of Arizona
Tucson, AZ

ABSTRACT

A newly developed nonlinear ultrasonic (NLU) technique called sideband band peak count-index (or SPC-I) measures the degree of nonlinearity associated with the inspected specimen – larger SPC-I values indicate higher nonlinearity. In various published papers, the SPC-I technique has shown its effectiveness and superiority in comparison to other techniques for nondestructive testing (NDT) and structural health monitoring (SHM) applications. In this work, the performance of SPC-I in non-homogeneous specimens having different topographies is investigated using peridynamics based periultrasound modeling. Three types of topographies - "X" topography, "Y" topography and "XY" topography are introduced by adding thin strips made up of a second material and thus converting the homogeneous plate into a heterogeneous structure. It is observed that "X" and "XY" topographies can help to hide the crack growth, thus making cracks undetectable to the nonlinear SPC-I based monitoring technique. In addition to the SPC-I technique, we investigate the applicability of the emerging method of topological acoustic sensing. This method monitors the changes in the geometric phase; a measure of the changes in linear or nonlinear wave's spatial behavior during its propagation in plate structures having various topographies. The computed results show that the magnitudes of jumps in geometric phase change plots can be good indicators to distinguish cracks with different thicknesses although these cracks can remain hidden in some topographies during the single point inspection based on the nonlinear SPC-I based monitoring technique.

Keywords: Nonlinear ultrasonic technique; SPC-I technique; peri-ultrasound modeling; topological acoustic sensing; geometric phase change; topography; structural health monitoring

1. INTRODUCTION

Nondestructive testing and evaluation (NDT&E) techniques using acoustic signals are widely used for structural health monitoring (SHM) for ensuring the safety of structural components' operation [1, 2]. Monitoring damages such as cracks in engineering structures is important. Various wellestablished acoustic techniques can monitor damage growth in homogeneous structures. However, when damages or cracks appear in heterogeneous structures having various topographies it becomes much more challenging. For simplicity we will call such structures having various topographies as "topographical structures". Topographical structures can be found in engineering applications, such as welded structures or when thinwalled ductile metallic plate structures are bent, topographies of the bent regions become different from the flat parts [3, 4]. Topographies in structures can result in complex wave interactions - reflections, refractions as well as negative wave interference when adopting acoustic wave-based monitoring techniques. When damages are generated in such topographical structures the damage-induced information can be destroyed by these negative effects. Therefore, it would be of great interest to investigate the effect of topography on damage monitoring. Such investigation can provide guidance for proposing optimal acoustics based techniques to detect and/or monitor damage growth in engineering structures.

In recent years nonlinear ultrasonic (NLU) techniques have become more popular than conventional linear ultrasonic (LU) based techniques due to their high sensitivities for monitoring damages at the early stage [5]. A newly developed NLU technique called sideband peak count – index (or SPC-I) has shown promising results for monitoring damages in different materials such as concrete [6-9], fiber reinforced polymer composite [10-12], metallic material [5, 13], fiber reinforced cement mortar [14, 15] and additively manufactured metal parts

[16, 17]. In the SPC-I technique, sideband peaks are counted above a moving horizontal threshold line as this line varies between a preset lower limit and an upper limit in the spectral plot. The SPC-I values measure the degree of nonlinearity associated with the inspected specimen – larger SPC-I values indicate higher nonlinearity. The SPC-I technique shows many advantages over other NLU techniques such as the two most popular and well-established techniques - higher harmonics generation (HHG) technique and nonlinear wave modulation spectroscopy (NWMS) method or frequency modulation (FM) method. For example, when adopting the HHG technique for guided waves propagating in plate structures, the guided wave mode selection criterion requires phase velocity and group velocity matching for the fundamental mode and the higher harmonic mode [18, 19], and for many engineering materials with complex internal structures such as composites and concretes the higher order harmonic components do not appear thus making it difficult to apply this technique. The NWMS/FM technique can be applied regardless of the material geometry or the presence of reflecting boundaries and structural inhomogeneity. However, the two input wave frequencies for wave mixing need to be precisely controlled for optimal sideband generation, which means narrow band excitation is needed [20]. The SPC-I technique does not have such restrictions and hence easier to implement, thus giving superiority to adopt the SPC-I technique for damage monitoring.

In general, damage monitoring related problems are challenging due to their complexities and uncertainties. It is almost impossible to monitor damage growth accurately from the experimental data extracted from received ultrasonic signals at one receiver. For more complex topographical structures, it is very difficult to conduct parametric analysis experimentally. Hence, a good numerical modeling method which can simulate elastic waves propagating and interacting with damages producing nonlinear response in complex structures such as topographical structures would be necessary. It can help us to understand the physical mechanism and provide useful guidance for practical experimental investigations [21]. Peri-ultrasound modeling which is based on nonlocal peridynamics theory [22, 23] has shown advantages over other numerical modeling methods for modeling elastic wave propagation and its interaction with cracks, producing nonlinear response. Compared to finite element method (FEM) based modeling (spring model and activating/deactivating elements) [24, 25] and finite difference based method such as local interaction simulation approach or LISA [26, 27], peri-ultrasound modeling can simulate nonlinear response from wave-crack interaction without changing cracks' surface properties artificially. It gives peri-ultrasound modeling advantages over other numerical methods. It should be noted that in finite element modeling when damage or crack sizes change, all meshes of elements and properties of cracked regions should be refreshed, element sizes become smaller, the number of elements increase rapidly, and it becomes challenging to artificially change the cracks' surface properties properly in these numerical methods. However, the mesh-free peri-ultrasound modeling does not have such

restrictions since horizon size in peridynamics theory is directly related to the particle size, any change in the particle size changes the horizon size automatically.

Combining peri-ultrasound modeling and SPC-I technique the structural damages have been monitored successfully. The peri-ultrasound modeling has been adopted for elastic wave propagating and interacting with cracks, thus producing nonlinear response in structures, and the SPC-I technique is then adopted as a nonlinear analysis tool to extract the nonlinear response from recorded peri-ultrasound modeling signals. Hafezi and Kundu [28-30] initialed the peri-ultrasound modeling concept based on bond-based peridynamics for modeling elastic waves propagating and interacting with single crack in twodimensional (2-D) plates, and nonlinear response was extracted with sideband peak count (SPC) technique - SPC plots for SPC-I analysis. It showed that thin cracks depict higher degree of nonlinearity than thick cracks and no cracks cases. Zhang et al [21, 31] investigated nonlinear response for multiple cracks in three-dimensional (3-D) plate structures using state-based periultrasound modeling, and definite relations between crack size ("thin" cracks and "thick" cracks) and horizon size which is mentioned in nonlocal peridynamics have been established. Similar nonlinear trends have been observed for multiple cracks cases – the SPC-I values for thin cracks are larger than that for thick cracks and no cracks cases. Dynamic propagation process of cracks and its monitoring with SPC-I technique has been also investigated combining peridynamics and peri-ultrasound modeling. SPC-I shows an increasing trend at the initial stages of crack propagation (when only thin cracks are generated) and then SPC-I values start to decrease as the loading increases (then thin cracks coalesce to form thick cracks) [32]. These investigations provide evidence that on one hand peri-ultrasound modeling is a useful tool for modeling nonlinear interactions between elastic waves and cracks, and on the other hand, the SPC-I technique is a promising tool to extract nonlinear response due to crack-induced nonlinearity.

In this work different thicknesses of stationary cracks which can present damage growth in topographical plate structures is investigated. Three types of topographies – "X" topography, "Y" topography and "XY" topography are considered in plate structures. Topographies are formed by inserting strips of a second material in different directions. Letters "X", "Y" and "XY" indicate the distribution directions of these strips ("X" indicates that strips are distributed along the x-axis, similarly "Y" for y-axis while "XY" implies the strips are distributed in both directions). The proposed peridynamics based periultrasound modeling is adopted to simulate elastic waves propagating and interacting with cracks in these topographical plate structures. Nonlinear responses which come from wavecracks interactions are captured and analyzed by the SPC-I technique to check the effect of different topographies on the crack detectability. An emerging concept - geometric phase which is from topological acoustic sensing is also investigated to help monitoring damage growth in topographical structures.

2. THEORY AND METHOD

In this section, basic theory and method which include crack-induced nonlinearity in the peri-ultrasound modeling framework and nonlinear ultrasonic SPC-I analysis for nonlinear response are only briefly introduced. The ordinary state-based (OSB) peri-ultrasound is adopted here for modeling elastic waves propagate and interact with cracks in topographical structures, and detailed theory and algorithm of OSB peri-ultrasound modeling can be found in the authors' previously published papers [21, 31, 32] thus here we omit repetitive illustrations for fundamental knowledge. Only the important part of SPC-I analysis is depicted here, and there are also many related both numerical and experimental investigations can be found in literatures as mentioned in introduction part so that one can refer to them if interested.

2.1 Crack-induced nonlinearity in peri-ultrasound framework

Though fundamental knowledge about OSB peridynamics can be found in the existing literature, investigations about OSB peri-ultrasound modeling are meager especially the crackinduced nonlinearity in structures. Therefore, it is still necessary to illustrate and provide detailed information for crack-induced nonlinearity in the peri-ultrasound framework. Figure 1 shows the partial schematic diagram for modeling ultrasonic waves propagating through cracks of different thickness using periultrasound modeling approach, and "thin" cracks and "thick" cracks are defined. The whole structure is divided into many cubes with side length Δx with one integration point at the center of each cube in peri-ultrasound modeling. The cracks are formed by artificially removing layers of cubes and can be classified as "thin crack" and "thick crack" as shown in figures 1b and 1c depending on the horizon radius δ mentioned in nonlocal peridynamics theory. The dashed line denotes the boundary of a crack in the structure, the integration point at the center of the circle, on the bottom side of the crack shown in figures 1b and 1c denotes the current calculation point. The corresponding point on the opposite side of the crack, which is the nearest point on the other side of the crack from the current integration point, is within the horizon circle of radius δ for a "thin crack" [figure 1b] and outside the circle for a "thick crack" [figure 1c].

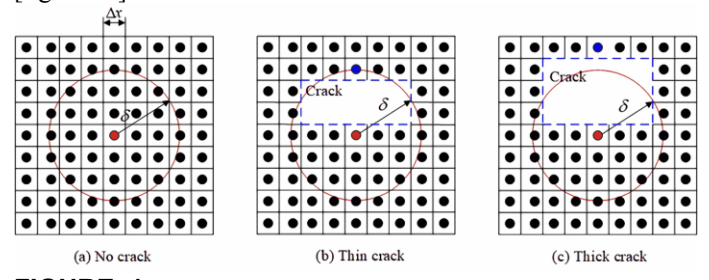


FIGURE 1: PARTIAL SCHEMATIC OF PERI-ULTRASOUND WAVE PROPAGATION MODELING THROUGH CRACKS OF DIFFERENT THICKNESS [21, 31]

In the nonlocal peri-ultrasound modeling, the cracks are modeled by removing material cubes and thus the overall stiffness of the region near the crack is also reduced. The nonlinearity arising from the interactions between the propagating elastic waves and cracks is captured indirectly through the interactions between the material points located on the two sides of a crack when the points are located within a horizon despite being separated by the crack as shown in figures 1b and 1c. Note that in pure linear elastic continuum model elastic waves cannot pass through any crack of finite thickness. When the crack thickness increases, the interactions between the points on the two sides of the crack decreases. In this manner the effect of the clapping phenomenon is indirectly captured since the clapping of thin cracks also allows more wave energy to pass through a thin crack compared to a thick crack. Thus, both peri-ultrasound modeling and crack clapping phenomenon result in more interactions between the points on the two sides of the crack for thin cracks compared to thick cracks.

2.2 Nonlinear SPC-I analysis method

Once signals generated by the peri-ultrasound modeling, mentioned in section 2.1 are recorded, the nonlinear parameter SPC-I is calculated. The details of sideband peak count—index (or SPC-I) can be found in earlier publications as suggested in Section 1. Here only key parts of the SPC-I analysis process is briefly described.

Consider a spectral plot generated from a recorded signal in a nonlinear structure as shown in the schematic diagram in figure 2a. The nonlinearities may be caused by damages or micro-cracks. Interactions between input elastic waves of different frequency (major peaks in figure 2a) produce additional small peaks when propagating through nonlinear materials due to the frequency modulation effect as shown in the spectral plot. In the SPC-I analysis we are interested in counting the peaks generated by the modulation effect.

The SPC plot shown in figure 2b is generated by counting the peaks above a moving threshold line, shown by the horizontal continuous line in figure 2a. The threshold line is moved vertically between two pre-set values which we call the lower threshold limit and upper threshold limit shown by the dashed lines. When the moving threshold line is varying vertically from the lower threshold limit to the upper threshold limit, all peaks shown by the circles that are above the moving threshold line are counted and plotted against the moving threshold value. The SPC plot (number of peaks as a function of the threshold value) gives a visual representation of the degree of material nonlinearity. A solid medium with high degree of nonlinearity should give higher SPC values compared to that for a linear elastic medium having a lower degree of nonlinearity.

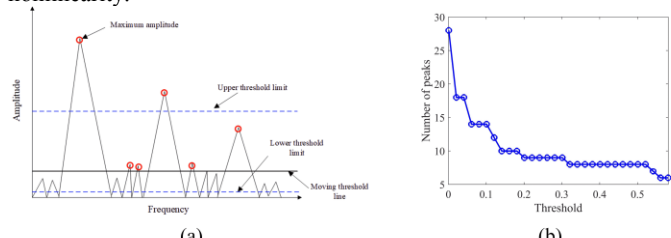


FIGURE 2: ILLUSTRATION OF SPC. (a) SIDEBAND PEAK COUNTING AND (b) EXAMPLE OF SPC PLOT [21, 31-33]

The SPC-I is an index value which is the average of SPC values for all threshold positions. This index indicates the degree of material nonlinearity, higher the material nonlinearity, greater is the number. In this work, we adopt the SPC-I for investigating crack-induced nonlinear response in different types of topographical structures.

3. MODEL DESCRIPTION

Plate structures containing two identical cracks with different thickness with and without topographies are investigated and compared to examine the effect of topography on the detectability of cracks in plate structures using the SPC-I technique. For no topography case, an isotropic steel plate is considered. Then topographic structures are formed by inserting thin strips made of aluminum in the steel plate, thus the topographic structure becomes heterogeneous. Three types of topography – "X" topography, "Y" topography and "XY" topography are considered. "X" and "Y" topographies indicate that these strips are inserted and arranged along x-axis and y-axis directions, respectively. For the "XY" topography the strips are inserted in both x- and y-axes directions.

3.1 Homogeneous plate structure

To investigate the effect of topography on the crack detection, for comparison first a homogeneous steel plate containing two cracks is considered. The 2-D view (in the xy plane) of the problem geometry is shown in figure 3. The dimension of the plate is $201 \times 201 \times 3$ mm³, and the steel material properties for numerical modeling are listed in Table 1 in section 3.2 along with the material properties of inserted aluminum strips. For wave propagation modeling, the vertical distance of the transmitting point and the receiving point from the x-axis is taken as 60 mm in opposite directions. Thus, these two points are located on the y-axis symmetrically about the x axis. Two identical cracks with length 19 mm and width d mm (d takes value 0, 1, 2 and 4 in this work) is considered for modeling damage growth. The two cracks are symmetrically placed about the x-axis and the closest vertical distance of the crack surface from the x-axis for each crack is 20 mm. Two cracks are also located symmetrically about the y-axis as shown in figure 3.

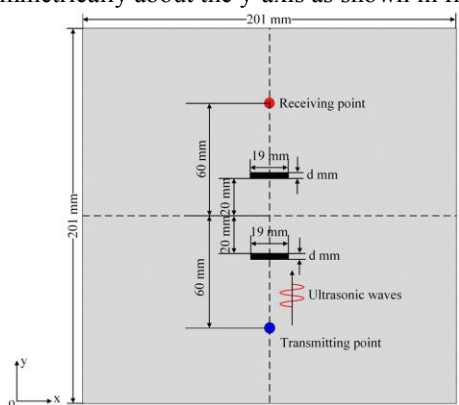


FIGURE 3: 2-D VIEW OF PROBLEM GEOMETRY FOR THE WAVE PROPAGATION MODELING IN A HOMOGENEOUS STEEL PLATE CONTAINING TWO CRACKS. THE THICKNESS D OF CRACKS CAN HAVE VALUES 0 MM (NO CRACK), 1 MM, 2 MM AND 4 MM TO MODEL DAMAGE GROWTH

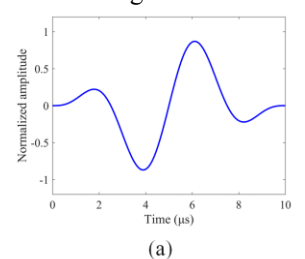
In the peri-ultrasound modeling the entire plate structure is discretized into cubes with side length 1 mm and cracks are formed by removing one or more layers of cubes from the plate structure. For example, each crack in figure 3 can be formed by removing d layers

(where d takes values 0, 1, 2 and 4 to model cracks of different thicknesses) of cubes in the y direction and in each layer 19 cubes in the x direction, 3 layers in the z direction are removed to form throughthickness cracks. The horizon size is selected as $\mathcal{S}=3.015\Delta x$ following references [21, 31, 32] to ensure both computational efficiency and accuracy, where Δx is 1 mm which denotes the side length of a cube as mentioned above.

An Hanning window modulated excitation displacement field (see equation 1) is applied at the transmitting point to excite the structure in the negative z direction.

$$u(\mathbf{x},t) = u_0(\mathbf{x})\sin(2\pi ft)\sin^2(\pi \frac{t}{T})$$
 (1)

In equation (1), f is the central frequency of the ultrasonic wave which is 200 kHz, t is time and T is the total duration of the excitation which can control the number of cycles of the input excitation signal. \mathbf{x} is a 3-D location vector that denotes the excitation point position at which the displacement field is applied (transmitting sensor position). u_0 is the initial displacement amplitude that takes value $1 \times 10^{-4} \mathrm{m}$ in our periultrasound modeling. The normalized time domain and frequency domain signals for the input or initial excitation are shown in figure 4.



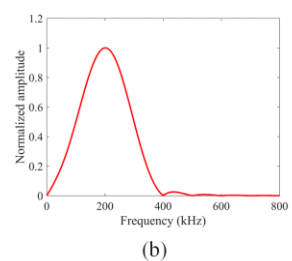


FIGURE 4: NORMALIZED INITIAL OR INPUT EXCITATION. (a) TIME DOMAIN SIGNAL AND (b) FREQUENCY DOMAIN SIGNAL

At the receiving point, out-of-plane velocity fields (in the z direction) for each crack thickness are recorded at each calculation step to obtain the history signal. The sampling frequency at the receiving point is 50 MSa/s (mega samples per second). Total 4 signals for crack thickness 0 mm (No crack), 1 mm, 2 mm and 4 mm are obtained for further SPC-I analysis.

3.2 Topographical structures – aluminum strips in the steel plate

For the same plate structure dimensions shown in figure 3, aluminum strips are inserted in steel matrix to form the heterogeneous topographical structure. Three types of topography – "X" topography, "Y" topography and "XY" topography are considered as shown in figure 5.

The "X" topography shown in figure 5a consists of two pairs of aluminum strips (four strips) inserted and arranged in the x-axis direction in the steel plate. Both pairs of strips are symmetrically arranged about the y-axis as shown in the figure.

The "Y" topography shown in figure 5b includes three aluminum strips arranged in the y-axis direction and inserted in the steel plate, one of which is located at the center of the plate with its central line coinciding with the x-axis, and the other two are symmetrically distributed about the x-axis, as shown in the figure.

The "XY" topography is simply the combinations of "X" topography and "Y" topography as shown in figure 5c. In each topography case, the width of the strips is the same which is 7 mm and their length is 201 mm which is equal to the side length of the square steel plate, as shown in the figure. Aluminum and steel properties for the peri-ultrasound modeling are shown in Table 1.

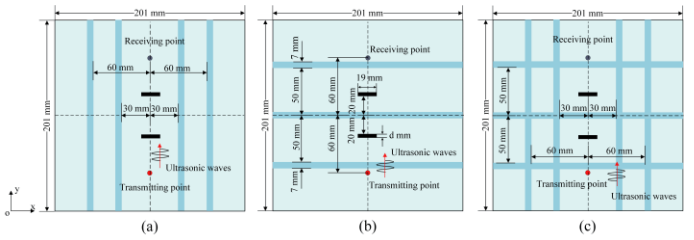


FIGURE 5: 2-D VIEW OF STEEL PLATES CONTAINING ALUMINUM STRIPS AND TWO CRACKS - (a) "X" TOPOGRAPHY, (b) "Y" TOPOGRAPHY AND (c) "XY" TOPOGRAPHY

TABLE 1: MATERIAL PROPERTIES OF ALUMINUM AND STEEL USED IN PERI-ULTRASOUND MODELING

Materials	Young's modulus	Poisson's	Density
	(GPa)	ratio	(kg/m^3)
Aluminum	71.50	0.33	2700
Steel	220.00	0.30	7800

To have a better understanding of how elastic waves propagate in topographical structures, the phase velocity dispersion curves of 3 mm thick steel plate and aluminum plate are computed using the material properties given in Table 1. Figure 6 shows these plots.

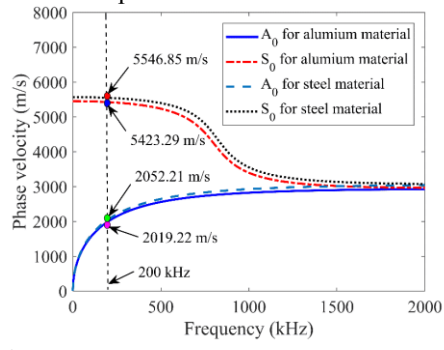
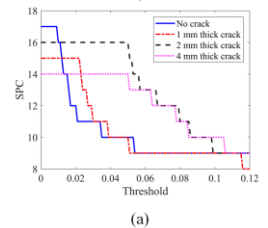


FIGURE 6: PHASE VELOCITY DISPERSION CURVES FOR ALUMINUM AND STEEL MATERIALS IN 3 MM THICK PLATE

4. SPC-I ANALYSIS RESULTS FOR CRACK DETECTION

4.1 Homogeneous steel plate – in absence of any topography

The SPC curves (number of peaks in the spectral plots above the moving threshold) and the SPC-I variations for different crack thicknesses are obtained following the steps described above, and the final results are shown in figure 7.



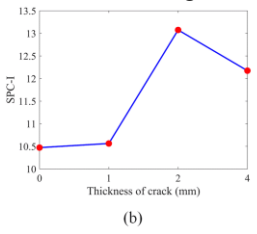


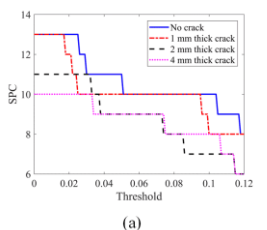
FIGURE 7: FOR THE HOMOGENEOUS STEEL PLATE, SHOWN IN FIGURE 3, CONTAINING TWO CRACKS WITH DIFFERENT THICKNESS VALUES - 0 MM (NO CRACK), 1 MM, 2 MM AND 4 MM, THE SPC PLOTS WITH THRESHOLD VARYING FROM 0 TO 12% OF THE MAXIMUM AMPLITUDES OF EACH SPECTRAL PLOT ARE SHOWN IN FIGURE 7(a) AND THE SPC-I VARIATION IS SHOWN IN FIGURE 7(b)

It can be seen that SPC-I shows an increasing trend up to 2 mm thick crack, and then starts to decrease. In several experimental and theoretical investigations this trend has been observed [8-10, 12, 21]. Such hump in the SPC-I plot indicates increasing level damage. In this case cracks becoming thicker.

4.2 Topographical plate structures – aluminum strips in steel plates

4.2.1 "X" topography

For the plate with X-topography (vertical aluminum strips placed in a steel plate) as shown in figure 5a, the SPC plots and the SPC-I variations are shown in figure 8.



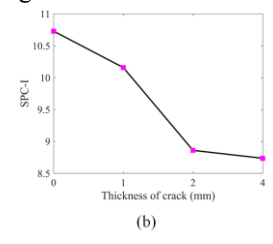


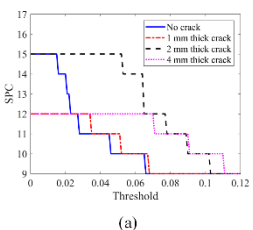
FIGURE 8: FOR THE TOPOGRAPHICAL PLATE CONTAINING TWO CRACKS OF DIFFERENT THICKNESSES AND HAVING "X" TOPOGRAPHY (VERTICAL ALUMINUM STRIPS IN A STEEL PLATE AS SHOWN IN FIGURE 5a) THE SPC PLOTS ARE SHOWN IN FIGURE 8(a) AND THE SPC-I VARIATION IS SHOWN IN FIGURE 8(b)

In this case, SPC-I variations show a completely different trend. Figure 8b shows monotonically decreasing trend. In absence of a hump in the SPC-I plot, that was observed in figure 7b, one cannot conclude the increasing level of damage. Therefore, the crack growth remains hidden in this topographical

structure. In other words, one may conclude that such "X" topography can help hiding the crack growth in plate structures and hinder its detection.

4.2.2 "Y" topography

For "Y" topography (shown in figure 5b), the SPC plots and the SPC-I variations for different crack thicknesses are shown in figure 9.



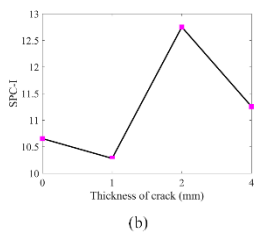
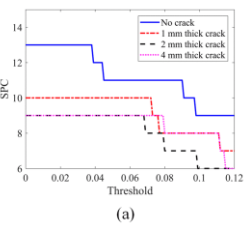


FIGURE 9: FOR THE TOPOGRAPHICAL PLATE CONTAINING TWO CRACKS OF DIFFERENT THICKNESSES AND HAVING "Y" TOPOGRAPHY (HORIZONTAL ALUMINUM STRIPS IN A STEEL PLATE AS SHOWN IN FIGURE 5b) THE SPC PLOTS ARE SHOWN IN FIGURE 9(a) AND THE SPC-1 VARIATION IS SHOWN IN FIGURE 9(b)

The SPC-I variation in figure 9(b) shows a hump having its peak for 2 mm thick crack as was the case for the homogeneous plate in figure 7(b). Therefore, the crack growth can be detected for the "Y" topography case.

4.2.3 "XY" topography

For "XY" topography (shown in figure 5c), the SPC plots and the SPC-I variations for different crack thicknesses are shown in figure 10.



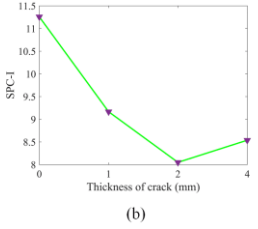


FIGURE 10: FOR THE TOPOGRAPHICAL PLATE CONTAINING TWO CRACKS OF DIFFERENT THICKNESSES AND HAVING "XY" TOPOGRAPHY (BOTH HORIZONTAL AND VERTICAL ALUMINUM STRIPS IN A STEEL PLATE AS SHOWN IN FIGURE 5c) THE SPC PLOTS ARE SHOWN IN FIGURE 10(a) AND THE SPC-I VARIATION IS SHOWN IN FIGURE 10(b)

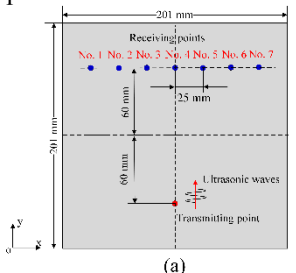
The SPC-I variation in figure 10(b) does not show any hump as was observed for the homogeneous plate in figure 7(b) or for "Y" topography as in figure 9(b). Therefore, the crack growth cannot be detected for the "XY" topography. Thus, one can conclude that "X" and "XY" topographies can hide the crack growth in plate structures and hinder its detection while "Y" topography does not do that.

5. TOPOLOGICAL ACOUSTIC SENSING ANALYSIS AND RESULTS

In this section, an emerging concept – geometric phase change based on topological acoustics is adopted. It is investigated whether those cracks that are hidden during SPC-I based monitoring can be detected through geometric phase change parameter from topological acoustic sensing technique.

The geometric phase concept which comes from the topological acoustic sensing can capture any change of wave propagation characteristics in a multi-dimensional space. The geometric phase changes due to topological structural change in multi-dimensional Hilbert space and this phase is different from dynamic phase concept (in time dependent signals). These geometric phase changes can be regarded as space invariants during wave propagation since they are only related to space perturbation introduced in the reference geometric shape [34]. and any changes in geometric phase correspond to the slight perturbation in reference geometric shape. Topological acoustic sensing with geometric phase has been investigated in the literatures and has been successfully applied for continuous monitoring of arctic forested areas using seismic waves [35, 36], sensing mass defects in coupled one-dimensional acoustic waveguides [37], analyzing dynamics of granular metamaterial [38] and underwater sensing for perturbation [39]. All these investigations adopted topological acoustic sensing with geometric phase and show that any simple change in space can cause sharp jumps in geometric phase. A sharp jump in geometric phase indicates high sensitivity of the geometric phase to that change. We investigate the capability of geometric phase change in detecting crack growth in both homogeneous plate and heterogeneous plates with various topographies.

For topological acoustic sensing, seven receiving points are considered as shown in figure 11. It should be noted that at least two receiving points are needed to reflect the space characteristics during wave propagation and more receiving points will improve the spatial resolution. Here, seven points are distributed symmetrically about the y-axis as shown in figure 11a (for the homogeneous plate without any crack) and in figure 11b (for the homogeneous plate with two cracks same as in figure 3). The geometric phase will change if there are any perturbations arising from these cracks. The thickness d of these two cracks takes values 0, 1, 2 and 4 for modeling damage growth in the plate. Plates having no crack is considered as the reference state or reference shape with respect to which the cracked cases are compared.



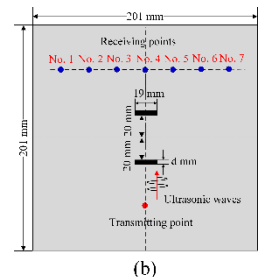


FIGURE 11: 2-D VIEW OF THE PROBLEM GEOMETRY FOR GEOMETRIC PHASE SENSING (a) CRACK-FREE REFERENCE STATE AND (b) CRACKED PLATE – PERTURBED STATE

For the reference shape at each receiving location we get a complex amplitude in the spectral plot from Fast Fourier Transform (FFT) of recorded time history signals, then a total of seven such complex amplitudes can be obtained. At a given frequency, these complex amplitudes of acoustic fields can be presented as a normalized state vector in a multi-dimensional Hilbert space whose 7 basis vectors correspond to locations in the physical space. This normalized state vector for reference geometric shape can be illustrated as [39],

$$C = \frac{1}{\sqrt{C_1^2 + C_2^2 + C_3^2 + \dots C_7^2}} \begin{pmatrix} C_1 e^{i\phi_1} \\ C_2 e^{i\phi_2} \\ C_3 e^{i\phi_3} \\ \dots \\ C_7 e^{i\phi_7} \end{pmatrix}$$
(2)

In equation (2), C_i and ϕ_i (i=1,2,3...7) are magnitude and spatial phase at each receiving point, when signals are received along different propagation paths. The components of this multi-dimensional state vector are the complex amplitudes of the field at every location in the physical space (plate structure here). Measuring the acoustic field at each discrete location in the physical space leads to a representation with a dimension equal to the number of points; so the dimension of the Hilbert space is 7 here. When cracks are introduced, the perturbation due to cracks in the physical space scatters the acoustic wave changes the normalized complex amplitude of the acoustic field to,

$$C' = \frac{1}{\sqrt{C_1'^2 + C_2'^2 + C_3'^2 + \dots C_7'^2}} \begin{pmatrix} C_1' e^{i\phi_1'} \\ C_2' e^{i\phi_2'} \\ C_3' e^{i\phi_3'} \\ \dots \\ C_7' e^{i\phi_7'} \end{pmatrix}$$
(3)

At a single given frequency f, one angle between the vector representation of the acoustic field along the 7 locations in the crack-free and cracked systems corresponds to a change in the geometric phase of the acoustic wave. This angle or single geometric phase change at given frequency f can be obtained through the dot product of these two state vectors and can be expressed as,

$$\Delta \varphi = \operatorname{arcos}(\operatorname{Re}(C^* \cdot C')), \quad \Delta \varphi \in [0, \pi]$$
 (4)

Where C^* denotes the complex conjugate of state vector C, while Re stands for the real part of a complex quantity, respectively.

Generally, the acoustic signals at each receiving point contain multiple frequencies, then a series of geometric phase changes can be plotted versus frequency to see how the geometric phase change $\Delta \varphi$ varies at each frequency to show spatial characteristics during wave propagation.

Effect of the crack growth in a homogeneous steel plate on geometric phase change variation is shown in figure 12.

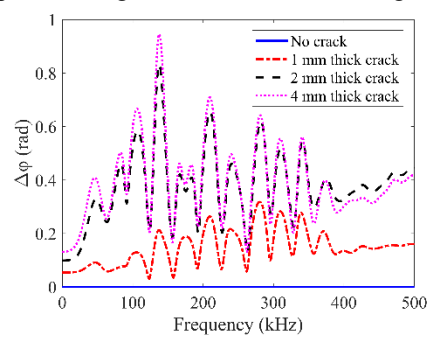


FIGURE 12: GEOMETRIC PHASE CHANGE AS A FUNCTION OF FREQUENCY AS THE CRACK THICKNESS INCREASES IN THE HOMOGENEOUS STEEL PLATE

The crack growth effect on the geometric phase change for plates having different topographies (X, Y and XY) are shown in figure 13.

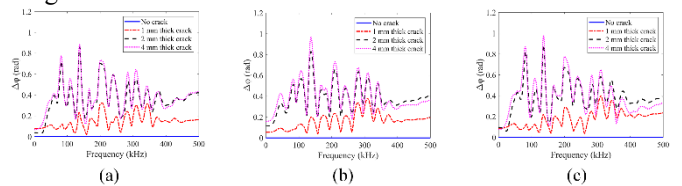


FIGURE 13: GEOMETRIC PHASE CHANGES AS A FUNCTION OF FREQUENCY AS THE CRACK THICKNESS INCREASES IN PLATES HAVING (a) "X" TOPOGRAPHY, (b) "Y" TOPOGRAPHY AND (c) "XY" TOPOGRAPHY

6. DISCUSSIONS

In all plots shown in figures 12 and 13 one can see that the introduction of cracks and crack thickness variations have strong effect on $\Delta\phi$ (the geometric phase change) for both the homogeneous plate and the plates with various topographies. At certain frequencies the $\Delta\phi$ change is stronger showing sharp peaks and dips compared to other frequencies. At higher frequencies (above 400 kHz) the oscillations in $\Delta\phi$ plot die down but it can still distinguish between no crack, 1 mm thick crack and 2 mm thick crack cases. However, no significant difference between 2 mm and 4 mm thick cracks is noticed. It should be noted here (see figure 7b) and in previous investigations [7, 10, 31] that SPC-I technique is more effective in sensing the initial stage of damage growth, and at higher frequencies $\Delta\phi$ is showing similar trends.

Comparison of figures 12 and 13 also show that "Y" topography in plate structures does not significantly affect the damage detection sensitivity since the "Y" topography results (figure 13b) are similar to no topography case (figure 12).

However, for "X" topography and "XY" topography (figures 13a and 13c) the $\Delta\phi$ variation patterns change from the homogeneous plate (figure 12) and "Y" topography (figure 13b) cases. We have seen earlier that for "X" and "XY" topographies the SPC-I does not show expected variation for crack growth and hence the cracks can remain hidden for these two topographies if the SPC-I values for one transmitter-receiver pair are used for their detection.

However, the geometric phase change parameter can be used for monitoring those cracks in topographical structures. Figure 13 shows that the magnitudes of jumps of $\Delta\phi$ increase with crack thicknesses for all three topographies – "X", "Y" and "XY" at several frequencies. The relative changes of these jumps are big enough to distinguish these cracks and thus making these cracks detectable and their growths monitorable.

7. CONCLUSIONS

This work is useful for monitoring the damage growth in complex topographical structures. For some topographies the damage growth can remain hidden to the SPC-I technique with single transmitter-receiver pair. However, geometric phase change obtained from multiple receivers can detect those cracks and monitor their growth. The peri-ultrasound modeling results combining geometric phase change and SPC-I techniques can provide a strong crack detection tool and new insight in experimental investigation for structural health monitoring of topographical structures.

ACKNOWLEDGEMENTS

This work is partially supported by the National Science Foundation sponsored "New Frontiers of Sound Science and Technology Center" at the University of Arizona (Grant No. 2242925). Some financial support provided by the Central South University (CSU) in China towards the first author's stay at the University of Arizona is also gratefully acknowledged.

REFERENCES

- [1] Kot P, Muradov M, Gkantou M, et al. Recent advancements in non-destructive testing techniques for structural health monitoring. Applied Sciences, 2021, 11(6): 2750.
- [2] Pallares F J, Betti M, Bartoli G, et al. Structural health monitoring (SHM) and Nondestructive testing (NDT) of slender masonry structures: A practical review. Construction and Building Materials, 2021, 297: 123768.
- [3] Zhang C, Li W, Deng M. Investigation of energy trapping effect for nonlinear guided waves in a topographical structure. Applied Acoustics, 2023, 214: 109694.
- [4] Yuan X, Li W, Deng M. Quantitative assessment of corrosion-induced wall thinning in L-shaped bends using ultrasonic feature guided waves. Thin-Walled Structures, 2023: 111493.
- [5] Zhang G, Li X, Li T, et al. Monitoring elastoplastic deformation in ductile metallic materials using sideband peak count-index (SPC-I) technique. Journal of Nondestructive Evaluation, Diagnostics and Prognostics of Engineering Systems, 2023: 1-15.

- [6] Alnuaimi H N, Sasmal S, Amjad U, et al. Monitoring Concrete Curing by Linear and Nonlinear Ultrasonic Methods. ACI Materials Journal, 2021, 118(3).
- [7] Basu S, Thirumalaiselvi A, Sasmal S, et al. Nonlinear ultrasonics-based technique for monitoring damage progression in reinforced concrete structures. Ultrasonics, 2021, 115: 106472.
- [8] Arumaikani T, Sasmal S, Kundu T. Detection of initiation of corrosion induced damage in concrete structures using nonlinear ultrasonic techniques. The Journal of the Acoustical Society of America, 2022, 151(2): 1341-1352.
- [9] Castellano A, Fraddosio A, Piccioni M D, et al. Linear and nonlinear ultrasonic techniques for monitoring stress-induced damages in concrete. Journal of Nondestructive Evaluation, Diagnostics and Prognostics of Engineering Systems, 2021, 4(4): 041001.
- [10] Alnuaimi H, Amjad U, Russo P, et al. Monitoring damage in composite plates from crack initiation to macro-crack propagation combining linear and nonlinear ultrasonic techniques. Structural Health Monitoring, 2021, 20(1): 139-150. [11] Alnuaimi H, Amjad U, Park S, et al. An improved nonlinear ultrasonic technique for detecting and monitoring impact induced damage in composite plates. Ultrasonics, 2022, 119: 106620.
- [12] Alnuaimi H N, Amjad U, Russo P, et al. Advanced non-linear ultrasonic sideband peak count-index technique for efficient detection and monitoring of defects in composite plates. Journal of Vibration and Control, 2023: 10775463231168228.
- [13] Liu P, Sohn H, Kundu T, et al. Noncontact detection of fatigue cracks by laser nonlinear wave modulation spectroscopy (LNWMS). NDT & E International, 2014, 66: 106-116.
- [14] Eiras J N, Kundu T, Bonilla M, et al. Nondestructive monitoring of ageing of alkali resistant glass fiber reinforced cement (GRC). Journal of Nondestructive Evaluation, 2013, 32: 300-314.
- [15] Sasmal S, Basu S, Himakar C V V, et al. Detection of interface flaws in Concrete-FRP composite structures using linear and nonlinear ultrasonics based techniques[J]. Ultrasonics, 2023, 132: 107007.
- [16] Liu P, Yang L, Yi K, et al. Application of nonlinear ultrasonic analysis for in situ monitoring of metal additive manufacturing. Structural Health Monitoring, 2023, 22(3): 1760-1775.
- [17] Park S H, Alnuaimi H, Hayes A, et al. Nonlinear acoustic technique for monitoring porosity in additively manufactured parts. Journal of Nondestructive Evaluation, Diagnostics and Prognostics of Engineering Systems, 2022, 5(2): 021008.
- [18] Lan Z, Li W, Deng M, et al. Combined harmonic generation of feature guided waves mixing in a welded joint. Wave Motion, 2023, 117: 103103.
- [19] Jiang C, Li W, Ng C T, et al. Quasistatic component generation of group velocity mismatched guided waves in tubular structures for microdamage localization. Available at SSRN 4398162.

- [20] Park S H, Kundu T. A modified sideband peak count based nonlinear ultrasonic technique for material characterization. Ultrasonics, 2023, 128: 106858.
- [21] Zhang G, Li X, Kundu T. Ordinary state-based periultrasound modeling to study the effects of multiple cracks on the nonlinear response of plate structures. Ultrasonics, 2023, 133: 107028.
- [22] Silling S A. Reformulation of elasticity theory for discontinuities and long-range forces. Journal of the Mechanics and Physics of Solids, 2000, 48(1): 175-209.
- [23] Silling S A, Epton M, Weckner O, et al. Peridynamic states and constitutive modeling. Journal of elasticity, 2007, 88: 151-184.
- [24] Martowicz A, Packo P, Staszewski W J, et al. Modelling of nonlinear Vibro-acoustic wave interaction in cracked aluminum plates using local interaction simulation approach[C]//6th European Congress on Computational Methods in Applied Sciences and Engineering, Vienna, Austria. 2012.
- [25] Delsanto P P, Scalerandi M. A spring model for the simulation of the propagation of ultrasonic pulses through imperfect contact interfaces. The Journal of the Acoustical Society of America, 1998, 104(5): 2584-2591.
- [26] Shen Y, Cesnik C E S. Modeling of nonlinear interactions between guided waves and fatigue cracks using local interaction simulation approach. Ultrasonics, 2017, 74: 106-123.
- [27] Shen Y, Cesnik C E S. Nonlinear scattering and mode conversion of Lamb waves at breathing cracks: An efficient numerical approach. Ultrasonics, 2019, 94: 202-217.
- [28] Hafezi M H, Alebrahim R, Kundu T. Peri-ultrasound for modeling linear and nonlinear ultrasonic response. Ultrasonics, 2017, 80: 47-57.
- [29] Hafezi M H, Kundu T. Peri-ultrasound modeling for surface wave propagation. Ultrasonics, 2018, 84: 162-171.
- [30] Hadi Hafezi M, Kundu T. Peri-ultrasound modeling of dynamic response of an interface crack showing wave scattering

- and crack propagation. Journal of Nondestructive Evaluation, Diagnostics and Prognostics of Engineering Systems, 2018, 1(1): 011003-011003-6.
- [31] Zhang G, Li X, Zhang S, et al. Sideband peak count-index technique for monitoring multiple cracks in plate structures using ordinary state-based peri-ultrasound theory. The Journal of the Acoustical Society of America, 2022, 152(5): 3035-3048.
- [32] Zhang G, Li X, Li T, et al. Ordinary state-based peri-ultrasound modeling for monitoring crack propagation in plate structures using sideband peak count-index technique. Journal of Sound and Vibration, 2024, 568: 117962.
- [33] Wang, M., Pau, A., Zhang, G. et al. Monitoring prestress in plates by sideband peak count-index (SPC-I) and nonlinear higher harmonics techniques. Nonlinear Dynamics 111, 15749–15766 (2023)
- [34] Banerjee S. Metamaterials in Topological Acoustics. CRC Press, 2023.
- [35] Lata T D, Deymier P A, Runge K, et al. Topological acoustic sensing of spatial patterns of trees in a model forest landscape. Ecological Modelling, 2020, 419: 108964.
- [36] Lata T D, Deymier P A, Runge K, et al. Topological acoustic sensing of ground stiffness: Presenting a potential means of sensing warming permafrost in a forest. Cold Regions Science and Technology, 2022, 199: 103569.
- [37] Lata T D, Deymier P A, Runge K, et al. Topological acoustic sensing using nonseparable superpositions of acoustic waves. Vibration, 2022, 5(3): 513-529.
- [38] Hasan M A, Deymier P A. Modeling and simulations of a nonlinear granular metamaterial: application to geometric phase-based mass sensing. Modelling and Simulation in Materials Science and Engineering, 2022, 30(7): 074002.
- [39] Lata T D, Deymier P A, Runge K, et al. Underwater acoustic sensing using the geometric phase. The Journal of the Acoustical Society of America, 2023, 154(5): 2869-2877.